INTERNATIONAL JOURNAL OF AUTOMOTIVE AND MECHANICAL ENGINEERING (IJAME)
ISSN: 2229-8649 e-ISSN: 2180-1606
VOL. 17, ISSUE 4, 8274 – 8282
DOI: https://doi.org/10.15282/ijame.17.4.2020.05.0625

ORIGINAL ARTICLE

Studies on Adhesive Wear Characteristics of Centrifugally Cast Functionally Graded Ceramic Reinforced Composite

K. Kartik Sriram, N. Radhika*, Manu Sam and S. Shrihari

Department of Mechanical Engineering, Amrita School of Engineering, Coimbatore, Amrita Vishwa Vidyapeetham, India – 641112.
*Phone: +91 94435 66174

ABSTRACT – Functionally graded material containing LM13 aluminium alloy as matrix and alumina as reinforcement (10 wt. %) was fabricated ($\Phi_{out}150 \times \Phi_{in}90 \times 100$ mm) by centrifugal casting. Samples were machined from the cylindrical cast along its longitudinal axis. Variation in hardness along the radial cross-sectional wall revealed 33.7% improvement at the outer periphery due to higher presence of alumina. This zone was preferred for dry sliding wear experiments, designed based on Taguchi L27 orthogonal array by varying the process parameters like sliding velocity, sliding distance and load using pin-on-disc tribometer. Analysis of variance revealed velocity as most influential wear factor, next to load. An optimal condition to minimise adhesive wear was determined at a load of 15 N, sliding velocity of 3.5 m/s and sliding distance of 1250 m. Scanning electron microscope analysis on abraded surfaces showed formation of tribolayer at high velocities and delamination at high loads.

ARTICLE HISTORY
Received: 3rd May 2020
Revised: 5th Nov 2020
Accepted: 1st Dec 2020

KEYWORDS
Functionally graded materials;
Adhesive wear;
Aluminium FGM;
Taguchi technique,
LM13;
Centrifugal casting

INTRODUCTION

Aluminium metal matrix composites (MMCs) have gained popularity in engineering applications over the years, owing to enhanced wear resistance and increased strength over pure metals. MMCs consist of base metal with reinforcements, that are usually metallic or ceramic particles or fibres dispersed throughout the material. Several applications may require an increased wear resistance only on a particular surface. Although surface treatment processes help to achieve these properties, manufacturing costs encountered are substantially high [1-4]. The use of functionally graded materials (FGMs) in these cases provides a cheaper solution to the problem, without any trade-offs between material properties and cost. FGMs are materials that incorporate the advantages of both monolithic metals and MMCs [5-6]. These materials provide the flexibility to the designer to tailor the required properties for specific industrial applications. This made them a popular advanced material among composites and eliminated the limitations of coatings, where a sharp or abrupt change in properties along the coated layer interface was replaced by smooth, continuous and gradient transition [7-8].

Several fabrication procedures were successful in producing FGMs, among them centrifugal casting method was recognised as the most convenient route to produce tubular FGMs. Studies revealed that the difference in density between the base metal and reinforcement particles aided to attain a smooth gradient transition from low to the high volume fraction of reinforcement particles across the radial direction [9-10]. Stir casting was predominantly used for the synthesis of MMCs. This, followed by a secondary stage of centrifugal casting, facilitates a gradient distribution along with the microstructure [11]. Aluminium, due to its low density, superior strength, excellent machinability, high wear and corrosion resistance, and low strength to weight ratio, was utilised as the best-chosen matrix material by researchers. Commonly used ceramic reinforcement types include oxides, carbides, borides and nitrides. Reinforcements like silicon carbide (SiC), aluminium oxide (Al_2O_3), titanium carbide (TiC) and boron carbide (B_4C) are the most preferred ones [12-13]. The experiments conducted on Al FGMs with SiC, Al_2O_3 and TiC reinforcements, fabricated by gradient slurry disintegration and deposition process revealed that the porosity and microhardness of the FGM has a direct relationship with the vol % of reinforcement particles [14-15]. Similarly, experiments conducted on LM25 with aluminium diboride (AlB_2) revealed an increase of up to 70% in Brinell hardness, with an 11% rise in the volume fraction of AlB_2 [16]. SiC and Al_2O_3 particulate reinforced aluminium FGM brake disc, fabricated by centrifugal casting was subjected to Grey regional analysis [17]. Samples were taken from different zones along the radial direction to determine the optimum frictional and wear parameters.

Components experiencing adhesive wear in several applications raised the priority and relevance of studying its tribological characteristics. Its importance with FGMs is considered inevitable, as it involves a combination of distinct materials. The pin-on-disc tribometer is a commonly employed experimental setup used to study adhesive wear [18,19]. Parametric influence during the tribological analysis of MMCs were validated using Taguchi's technique, which are a crucial tool for the design of high-quality systems. Analysis of variance (ANOVA) and signal-to-noise ratio (S/N ratio) tools were utilised for optimisation of wear response parameters and identifying the most influential wear process

*CORRESPONDING AUTHOR | N. Radhika | ✉ n_radhika1@cb.amrita.edu

parameter respectively [20]. Wear parameters are variable individually or in combination, providing clear results to be used for statistical analysis. This analytical technique helps to optimise performance, quality and cost [21]. Wear response and friction were optimised in a comparative tribology study of Al/Si_3N_4 nanocomposite and Al/Gr/Si_3N_4 hybrid composite using ANOVA to determine sliding distance as the most influential factor (45.63%) on the rate of wear, next to applied load (43.39%) [22].

Extensive studies were carried out in the area of adhesive wear for MMCs but are limited for FGMs. Despite the potential applications of LM13 and Al_2O_3, its dry sliding wear behaviour as an FGM was yet not been studied. Therefore, this research is primarily focused on bridging this gap by statistically exploring the tribo-performance of the material developed and to the study the influential parametric combination that optimises wear.

MATERIALS AND METHODS

LM13, an aluminium alloy with a density of 2.7g/cm^3, has widespread applications in the automotive industry owing to its low coefficient of thermal expansion, high wear resistance and excellent weight-bearing properties. Being a material that is largely used in piston cylinders, piston rings, and engine blocks, it undergoes adhesive wear mechanism largely. The elemental composition of LM13 is mentioned in Table 1.

Table 1. Elemental composition of LM13 alloy.

Element	Percentage (%)
Al	83.39
Si	10.9
Fe	0.53
Cu	1.31
Mg	1.05
Ni	1.88
Others (Mn,Cr,Zn,Sn,Ti,Pb,Ca)	0.94

Spherical Al_2O_3 (10 wt.%) reinforcement particles with a density of 3.95 g/cm^3 and an average size of 10 µm were used as reinforcements, as it exhibited better wear-resistant properties. LM13/10wt.%Al_2O_3 was cast as a functionally graded material to concentrate the reinforcement particles near the outer periphery, where maximum wear occurs. The presence of ceramics was limited within the range of 5-10 wt.% for functionally graded composites. This is due to the lack in homogeneity at <5 wt.% and clustering effect at >10 wt.% [23-25].

Fabrication of Composite

Horizontal centrifugal casting is considered as a most feasible fabrication method to implement the FGM concept, as it is capable of producing a gradient microstructure based on the density difference between the ceramics and aluminium matrix [26]. The stir casting process was carried out at the pre-stage to ensure that reinforcement particles were distributed uniformly in the molten material before being poured into the centrifugal casting die. LM13 aluminium alloy ingots were melted using an electrical resistance furnace (Figure 1) in an inert argon gas atmosphere. A hopper was used to add pre-heated (200 ºC) Al_2O_3 particles into the crucible while stirring the molten metal at 300 rpm. Pre-heating the ceramics before addition to molten metal, helped to overcome the wettability challenge. Then this molten material was poured into the centrifugal casting machine's pre-heated steel die (350ºC), shown in Figure 2(a). The die, connected to the motor through a belt and pulley system was rotating at 1000 rpm, producing a centrifugal force, which drove the higher density particles towards the outer periphery. A cast hollow cylindrical component (Figure 2b), with an outer diameter of 150 mm, an inner diameter of 90 mm and length of 100 mm was obtained after solidification.

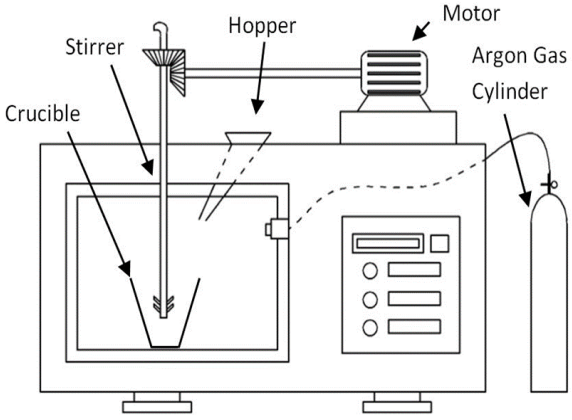

Figure 1. Electrical resistance furnace.

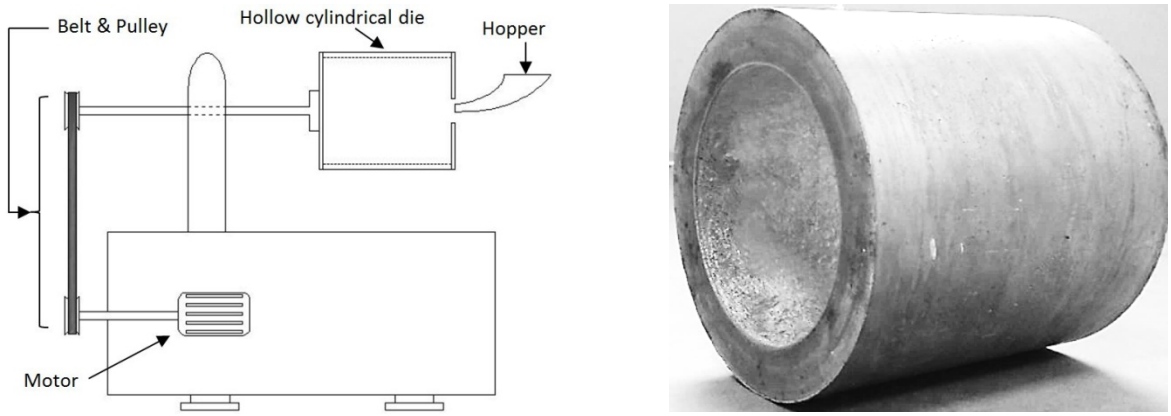

Figure 2. (a) Centrifugal casting machine schematic (b) Centrifugally cast product.

Hardness Testing

The presence of hard reinforcement particles influences the composite hardness to a substantial extent. The FGM specimen fabricated using horizontal centrifugal casting method was subjected to Vickers hardness testing, in order to ensure that the desired spatial variation in properties has been realised. Measurements were made according to ASTM E384 standard using a Mitutoyo Indentec Vickers hardness tester equipped with diamond indenter (pyramid shape). The test specimen was prepared by grinding using a bench grinder, followed by a Linisher polisher. Emery sheets of 1/0, 2/0, 3/0 and 4/0 grades were used to polish the surface further. Finally, a mirror-like finish was obtained using a double disc polishing machine.

In the Vickers hardness tester, the test piece was kept perpendicular to the direction of loading on an anvil with a screw-threaded base. The indenter has inverted, square-base pyramid made of diamond. The anvil was raised by turning the screw threads until the specimen was close to the indenter. The specimen was loaded with 500 gf for 15 sec using the indenter. After the loading process, the anvil was lowered, and the indentation on the surface was observed. The diagonal lengths, which are characterised by a pair of dark lines, were measured. Three values of hardness at the same distance from the outer wall zone were measured, and the mean value was calculated. The test was carried out at various radial distances from the outer wall zone. The radial variation in hardness from the outer wall zone is shown in Figure 3.

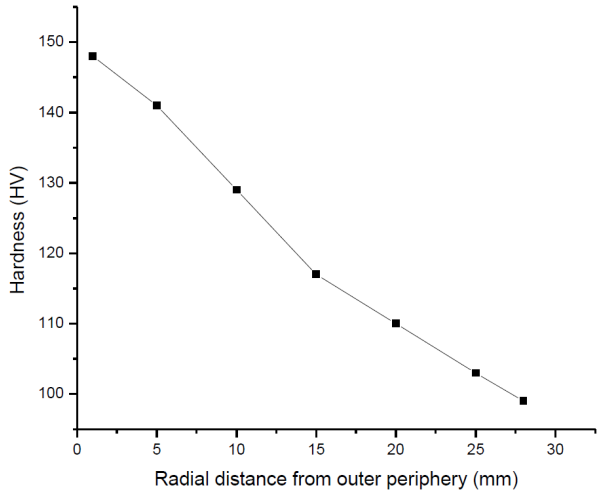

Figure 3. Variation of hardness along the radial direction from the outer periphery.

The hardness value was observed to increase gradually along the radial direction towards the outer radial wall. The particle-rich zone was observed near the outer wall, showing the highest hardness value (148 HV). During fabrication of the FGM through centrifugal casting technique, the higher-density reinforcement particles tend to segregate towards the outer periphery. This was due to the density difference at the particle-matrix interface, and also due to the centrifugal force created during the process. The low-density gas bubbles generated near the outer periphery were pushed towards the inner surface due to buoyancy. During this motion of gas bubbles, a low fraction of Al_2O_3 particles were attached to these bubbles and underwent a backward flow. This resulted in an increasing gradient distribution from inner to outer wall zone of the composite. This gradient in the concentration of reinforcement particles had a direct influence over the hardness values observed. Since the outer surface was found to be harder with a higher volume fraction of ceramic particles, it was chosen as the preferred surface to carry out wear experiments. Gradation of ceramic reinforcements across

the composite wall and their advantageous effect of providing superior mechanical properties were reported by many researchers [27-28].

Design of Experiment

The experiment was planned using Taguchi's design, and L_{27} Orthogonal array was preferred for optimising the number of experiments. The three parameters, sliding velocity, sliding distance and load, were varied on three levels, as shown in Table 2. The wear rate was evaluated using the signal to noise ratio and analysis of variance.

Table 2. Range of process parameters.

Levels	Load (N)	Velocity (m/s)	Distance (m)
1	15	1.5	750
2	25	2.5	1250
3	35	3.5	1750

Adhesive Wear Test

Pin specimens of 10×10×25 mm dimensions were prepared from the centrifugally cast component. Dry sliding wear tests were conducted on the surface from the outer wall zone of the composite, using a DUCOM TR-20LE pin-on-disc tribometer (Figure 4) as per ASTM G99 standards. Wear test parameters for experiments were fixed based out of the range prescribed on ASTM G99 standards. Trial experiments were conducted to identify the minimum threshold value for process parameters to identify sufficient wear. Each trial was repeated three times for confirmation and average inference.

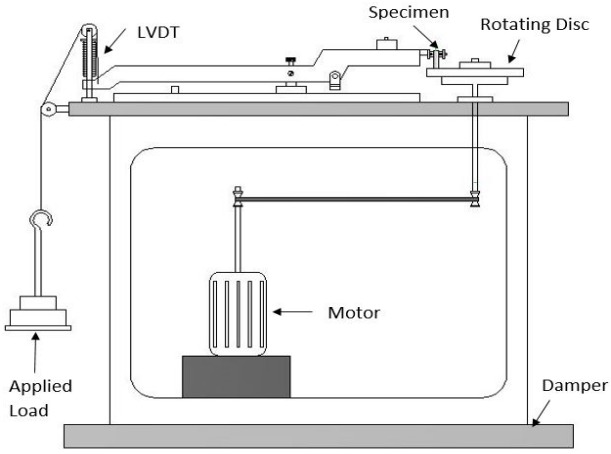

Figure 4. Pin-on-disc tribometer.

Based on the hardness test, the periphery with the highest hardness (highest concentration of reinforcement particles) was held against the rotating EN-32 steel disc of 65 HRC hardness. The track diameter was set to 80 mm and was used throughout the experiments. Weights were added to one end of the cantilever beam, in effect exerting the same load on the specimen against the rotating disc. The load applied, kept the specimen in contact with the disc throughout the experimental cycle. Wear led to a slight reduction in the dimension of the specimen, resulting in the displacement of the lever arm orthogonal to the wear surface. This caused the displacement of the lever arm, which was then measured by a Linear Variable Differential Transducer (LVDT) affixed to it. The specimen was properly cleaned and weighed before and after the experiments, using a micro-balance with least count of 0.1 mg. The difference in the mass of the specimen was measured and converted into volume loss using the density. The wear rate was calculated from volume loss using Eq. (1).

$$W = \frac{M}{\rho D} \tag{1}$$

where W is the rate of wear (mm^3/m), M is the reduction in mass (g), ρ is the specimen density (g/mm^3) and D is the sliding distance (m).

RESULTS AND DISCUSSION

Analysis of Signal-to-Noise Ratio

The wear rates were calculated from the experiments and are tabulated below in Table 3. It also shows their corresponding S/N ratios calculated using the statistical analysis software Minitab. The S/N ratio condenses effect of noise levels and repetitions into a single point data depending on the characteristic equation being evaluated. The

characteristic equation is divided into three categories, namely 'Smaller-the-better', 'Larger-the-better' and 'Nominal-is-the-best'. The process parameters were ranked according to their influence using the S/N ratio. The wear rate response table for S/N ratio is shown in Table 4. In this study "Smaller-the-better" characteristic equation of S/N ratio was considered, whose Eq. (2) is given by:

$$S/N = -10 \log \frac{1}{n} \left(y_1^2 + y_2^2 + \ldots + y_n^2 \right) \quad (2)$$

The difference between the maximum and minimum average S/N ratios for each factor was used to calculate the delta values. The parameters were further ranked, according to the descending order of delta value. From Table 4, it is evident that velocity was the major factor influencing wear rate, next to load and distance, respectively.

Table 3. L_{27} Orthogonal array and its wear experimental results.

S. no	Process parameters			Wear rate (mm^3/m)	S/N ratio (db)
	Load (N)	Velocity (m/s)	Sliding distance (m)		
1	15	1.5	750	0.001482	56.3697
2	15	1.5	1250	0.001185	58.0882
3	15	1.5	1750	0.00127	58.5775
4	15	2.5	750	0.000988	62.2793
5	15	2.5	1250	0.000889	59.9713
6	15	2.5	1750	0.000635	62.8257
7	15	3.5	750	0.000988	58.1519
8	15	3.5	1250	0.000593	66.0324
9	15	3.5	1750	0.000635	64.4139
10	25	1.5	750	0.001975	53.3015
11	25	1.5	1250	0.00237	54.1866
12	25	1.5	1750	0.002751	50.312
13	25	2.5	750	0.000494	63.9847
14	25	2.5	1250	0.001185	60.8433
15	25	2.5	1750	0.001058	59.3338
16	25	3.5	750	0.001482	59.516
17	25	3.5	1250	0.000296	66.5632
18	25	3.5	1750	0.001058	60.5807
19	35	1.5	750	0.002469	53.1513
20	35	1.5	1250	0.002074	52.4164
21	35	1.5	1750	0.002751	51.4542
22	35	2.5	750	0.000988	60.0799
23	35	2.5	1250	0.001482	55.3185
24	35	2.5	1750	0.001693	56.7214
25	35	3.5	750	0.001482	55.6115
26	35	3.5	1250	0.001185	61.0387
27	35	3.5	1750	0.001058	57.9686

Table 4. Wear rate response table for S/N ratio.

Level	Load (N)	Velocity (m/s)	Distance (m)
1	60.75	54.21	58.05
2	58.74	60.15	59.38
3	55.97	61.1	58.02
Delta	4.77	6.89	1.36
Rank	2	1	3

Parametric Influence on Wear Behaviour

The effect of influential factors on wear rate was evaluated using S/N ratios. Figure 5 shows the optimum level of parameters. It is seen that the wear resistance of composites was optimised at a minimum load of 15 N, the maximum sliding velocity of 3.5 m/s and a sliding distance of 1250 m. Figure 6 shows the mean plot of the wear response, where the wear rate is considered as the wear response in this analysis.

Applied Load on Wear Response

It is inferred from the graph of Figure 6(a) that rate of wear increases with the rise in load from 15 N to 35 N. At a low load of 15 N, the contact pressure at the sliding interface is low which leads to lower wear rate. The increase in the rate of wear at higher load, reveals plastic deformation of developed composite material. At the high loads of 25 N and 35 N, the temperature at the sliding interface of specimen and disc increases. This rise in temperature leads to softening

of the base metal and results in the adherence of pin material to the disc. This increases the wear rate of the specimen significantly. A similar inference was observed in a study, where the rate of wear tends to raise with increasing load. This is due to the higher presence of particles at the sliding surface, where the rate of change of wear decreases [29].

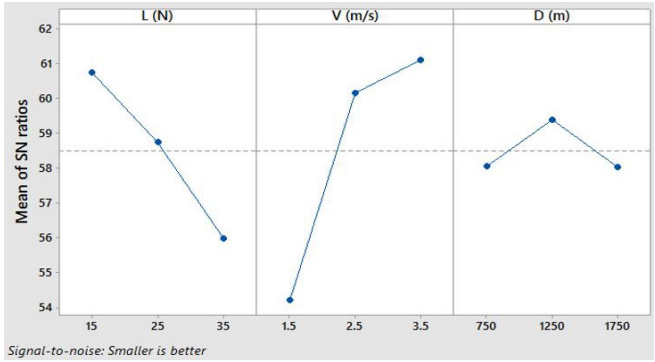

Figure 5. Plot showing the mean effect of S/N ratios.

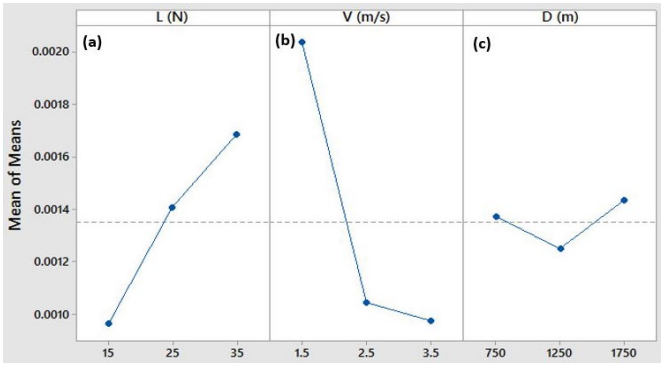

Figure 6. Plot showing the mean effect of means.

Sliding Velocity on Wear Response

The wear rate tends to decrease with rising in sliding velocity, as shown in Figure 6b. It is also seen that there is a sharp decrease in the rate of change in wear rate from 1.5 to 2.5 m/s. This is attributed to the formation of tribolayer. It is an innate quality of aluminium to form a protective oxide layer on the periphery exposed to the atmosphere. The temperature at the contact surface increased when sliding at high velocity (2.5 m/s), leading to oxidation of the specimen. This phenomenon leads to the transfer of materials from both contact surfaces, producing wear debris and eventually forming a mechanically mixed layer (MML), also known as a tribolayer. The tribolayer layer acts as a barrier, lubricating the contact surface and preventing further wear [30]. Moreover, at high velocities (of 2.5 m/s to 3.5 m/s) the MML formed stabilises, which decreases the rate of change of wear rate and improves the wear resistance of the FGM.

Sliding Distance on Wear Response

Rate of wear initially decreases for a sliding distance between 750 m and 1250 m, as shown in Figure 6(c). The decrease in trend is attributed to the presence of hard asperities at the periphery of the composite. These asperities reduced contact area, resulting in high initial wear rate (750 m). With increasing sliding distance (of 750 m to 1250 m), these asperities tend to get compacted between the periphery and disc, thereby becoming blunt. This increases the contact area and decreases the rate of wear [31]. The increasing trend from 1250 m to 1750 m is due to the increase in interfacial temperature caused by prolonged wear. This softens the composite and exhibits a higher rate of wear when slide against a harder material (EN32 disc).

Analysis of Variance

Analysis of variance (ANOVA) helps to analyse the influence of wear process parameters and their interaction on the wear response. Here, ANOVA helps to ascertain which process parameter among load, sliding distance, sliding velocity, and its interactions affect the performance characteristics significantly. ANOVA was determined for a 95% confidence level for wear rate. The p-value less than 0.05 indicates that the process parameter has a significant effect on the process. The results of ANOVA are tabulated in Table 5.

It is seen from the last column of Table 5 that the process parameter that has major control over the wear rate was velocity, V (at 53.85%), followed by the load, L (at 20.51%). Sliding distance, D (at 1.71%) had the lowest influence on the process. Load and velocity had a statistically significant effect on the process since its p-values were less than 0.05.

Table 5. ANOVA for wear rate.

Source	DF	Seq SS	Adj SS	Adj MS	F	P	Percentage
L	2	0.0000024	0.0000024	0.0000012	13.68	0.003	20.51
V	2	0.0000063	0.0000063	0.0000032	36.1	0	53.85
D	2	0.0000002	0.0000002	0.0000001	0.89	0.447	1.71
L*D	4	0.0000003	0.0000003	0.0000001	0.92	0.499	2.56
V*D	4	0.0000009	0.0000009	0.0000002	2.59	0.118	7.69
L*V	4	0.0000009	0.0000009	0.0000002	2.51	0.124	7.69
Error	8	0.0000007	0.0000007	0.0000001			5.98
Total	26	0.0000117					100

*Note: DF : Degree of Freedom, Seq SS : Sequential Sum of square, Adj SS : Adjusted Sum of Square, Adj MS : Adjusted mean Square, F : Fisher's test statistic, P : Probability

Linear Regression Model

The regression equation generated from Minitab software to validate the experimentally obtained wear rate is given below,

$$W=0.00044+0.000281*V+0.000044*L-0.000015*L*V \quad (3)$$

It is seen from Eq. (3) that the wear rate is independent on sliding distance, the interaction of sliding distance – load and interaction of sliding distance – velocity, as their respective coefficients in the regression model are zero. The final step of Taguchi analysis is conducting confirmation tests. The tests were done using a specific combination of levels and process parameters to validate the regression equation obtained. The parameter values chosen for the confirmation experiments were different from the values selected while planning experiments based on L_{27} orthogonal array. The results of the confirmatory experiments are shown in Table 6.

Table 6. Regression model for confirmatory wear rate tests and comparison.

Test No.	Load (N)	Sliding velocity (m/s)	Sliding distance (m)	Exp. wear rate (mm^3/m)	Regression wear rate (mm^3/m)	Error (%)
1	17	1.8	1000	0.0013342	0.0012348	7.4502
2	20	2.1	1400	0.0011932	0.0012801	7.2829
3	30	2.9	1700	0.0011890	0.0012699	6.8040

On analysing the data from Table 6, it is observed that the error between the values obtained from the regression equation and the experiment is less than 8%. Therefore, the model is reliable and effective to evaluate the dry sliding wear behaviour of the composite.

Scanning Electron Microscope Analysis

The mechanism of wear was analysed through the scanning electron microscope (SEM), conducted over the worn surface of the composite. Figure 7(a) and Figure 7(b) show the worn surfaces for sliding velocities of 1.5 m/s and 3.5 m/s respectively for a constant load of 25 N and sliding distance of 1250 m. It is observed from Figure 7(a) that the surface has predominantly undergone adhesion at low velocities. Breaking this local adhesion causes work hardening and initiation of cracks at the periphery, which further propagates and breaks, causing metal removal through delamination [32]. From Figure 7(b), the formation of MML is evident when the sliding velocity increased from 1.5 m/s to 3.5 m/s. The temperature at the sliding surface increases at high sliding velocities, which then causes oxidation of aluminium and material transfer from the pin towards the disc. This leads to the formation of MML, which reduces the material removal rate.

Figure 7(c) and Figure 7(d) show that the worn surface for loads 15 N and 35 N respectively, for a constant sliding distance of 1250 m and sliding velocity of 2.5 m/s. Figure 7(c) reveals shallow grooves at the low load (of 15 N), which undergo a further transition into deeper grooves at higher loads of 35 N, as seen in Figure 7(d). Delamination and ploughing are also evident from the abraded surface at high load. This deteriorates the tribological properties of the FGM. Figure 8 shows the worn periphery at the optimum condition. The abraded surface shows minimal scratches and grooves along the sliding direction, in addition to the formation of MML. Moreover, the scratches and grooves are shallower than the ones at other conditions.

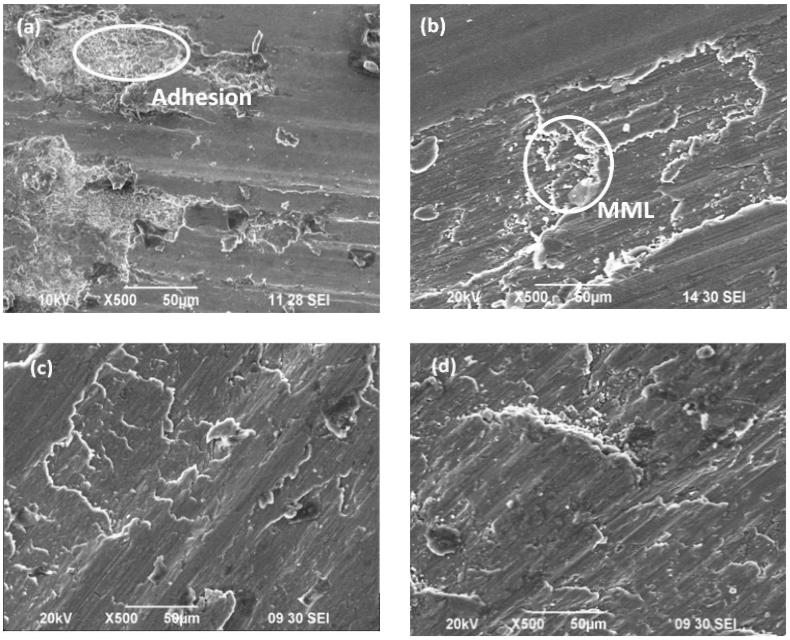

Figure 7. Worn surfaces at velocities of (a) V=1.5 m/s and (b) V=3.5 m/s and loads (c) L=15 N and (d) L=35 N.

Figure 8. Worn surface at the optimum level (L=15 N, V=3.5 m/s and D=1250 m).

CONCLUSION

Centrifuge cast LM13 aluminium FGM reinforced with 10 wt.% of Al_2O_3 particles was successfully fabricated with an increasing gradient of concentration of Al_2O_3 particles along the outward radial wall direction. This was then validated using the Vickers hardness test, which showed supreme hardness (of 148 HV) at the outermost wall zone confirming the higher presence of ceramic content at this zone. Therefore, this zone was preferred to conduct the adhesive wear experiments. Analysis of wear results revealed an increase in the rate of wear with a rise in load and a decrease in the rate of wear with increasing velocity. ANOVA results showed that velocity was the major factor, next to load in determining the wear response. Analysis of S/N ratios revealed optimal tribological properties at low load (10 N) and high sliding velocity (of 3.5 m/s). A multiple linear regression model was developed for the rate of wear. It was validated with the confirmatory experiments, and the errors were less than 8%. SEM analysis revealed adhesion at low velocities and the formation of a tribolayer at high velocities, which improved wear characteristics of the FGM. The tribological properties ascertained through this study are used for comparing and selecting appropriate composites. Developed FGM composite with supreme mechanical and tribological performance are used for automotive applications like engine piston, cylinder, pushrods, pumps, compressors, connecting rods, brake discs etc.

REFERENCES

[1] Adebisi AA, Maleque MA, Rahman MM. Metal matrix composite brake rotor: historical development and product life cycle analysis. International Journal of Automotive and Mechanical Engineering 2011; 4(1): 471-480.

[2] Hammood HS, Irhayyim SS, Awad AY, Abdulhadi HA. Influence of multiwall carbon nanotube on mechanical and wear properties of copper–iron composite. International Journal of Automotive and Mechanical Engineering 2020; 17(1): 7570-7576.

[3] Sam M, Radhika N. Comparative study on reciprocal tribology performance of mono-hybrid ceramic reinforced Al-9Si-3Cu graded composites. Silicon 2020; 3: 1-7.

[4] Sanuddin A, Ali A, Hanim MA. Fabrication of Al/Al2O3 FGM rotating disc. International Journal of Automotive and Mechanical Engineering 2012; 5: 622-629.

[5] Karimzadeh A, Aliofkhazraei M, Rouhaghdam AS. Study on wear and corrosion properties of functionally graded nickel–cobalt–Al2O3 coatings produced by pulse electrodeposition. Bulletin of Materials Science 2019; 42(2): 53.

[6] Naebe M, Shirvanimoghaddam K. Functionally graded materials: A review of fabrication and properties. Applied Materials Today 2016; 5: 223-245.

[7] Vencl A, Bobic I, Arostegui S, Bobic B, Marinković A, Babić M. Structural, mechanical and tribological properties of A356 aluminium alloy reinforced with Al2O3, SiC and SiC+ graphite particles. Journal of Alloys and Compounds 2010; 506(2): 631-639.

[8] Manu S, Radhika N. Wear and friction study of centrifugally cast functionally graded Cu-Ni-Si alloy and composite. Tribology in Industry 2020; 42(2).

[9] Jayakumar E, Praveen AP, Rajan TP, Pai BC. Studies on tribological characteristics of centrifugally cast SiCp-reinforced functionally graded A319 aluminium matrix composites. Transactions of the Indian Institute of Metals 2018; 71(11): 2741-8.

[10] Saiyathibrahim A, Subramanian R, Samuel CS. Processing and properties evaluation of centrifugally cast in-situ functionally graded composites reinforced with Al3Ni and Si particles. Materials Research Express 2019; 6(11): 1165a8.

[11] Ebhota WS, Karun AS, Inambao FL. Centrifugal casting technique baseline knowledge, applications, and processing parameters: overview. International Journal of Materials Research 2016; 107(10): 960-969.

[12] Sharma P, Sharma AK. Harmonic analysis of Al/Al2O3 and Ti-6Al-4V/aluminium oxide functionally graded plate. Materials Today: Proceedings 2017; 4(2): 1716-1722.

[13] Umanath KP, Palanikumar K, Selvamani ST. Analysis of dry sliding wear behaviour of Al6061/SiC/Al2O3 hybrid metal matrix composites. Composites Part B: Engineering 2013; 53:159-68.

[14] Babu KV, Jappes JW, Rajan T, Uthayakumar M. Dry sliding wear studies on SiC reinforced functionally graded aluminium matrix composites. Journal of Materials: Design and Applications 2014; 20(1): 57-67.

[15] Dhanasekaran S, Sunilraj S, Ramya G, Ravishankar S. SiC and Al2O3 reinforced aluminum metal matrix composites for heavy vehicle clutch applications. Transactions of the Indian Institute of Metals 2016; 69(3): 699-703.

[16] Arunagiri KS, Radhika N. Studies on adhesive wear characteristics of heat treated aluminium LM25/AlB2 composites. Tribology in Industry 2016; 38(3): 277-285.

[17] Radhika N, Balaji TV, Palaniappan S. Studies on mechanical properties and tribological behavior of LM25/SiC/Al2O3 composites. Journal of Engineering Science and Technology 2015; 10(2): 134-144.

[18] Watanabe Y, Kawamoto A, Matsuda K. Particle size distributions in functionally graded materials fabricated by the centrifugal solid-particle method. Composites science and Technology 2002; 62(6): 881-888.

[19] Ebhota WS, Karun AS, Inambao FL. Principles and baseline knowledge of functionally graded aluminium matrix materials (FGAMMs): Fabrication techniques and applications. International Journal of Engineering Research in Africa 2016; 26: 47-67.

[20] Radhika N, Senapathi SB, Subramaniam R, Subramany R, Vishnu KN. Pattern recognition based surface roughness prediction in turning hybrid metal matrix composite using random forest algorithm. Industrial Lubrication and Tribology 2013; 65(5): 311-319.

[21] Sivasankaran S, Ramkumar KR, Al-Mufadi FA, Irfan OM. Effect of TiB2/Gr hybrid reinforcements in Al 7075 matrix on sliding wear behavior analysed by response surface methodology. Metals and Materials International 2019; 1:01-17.

[22] Ambigai R, Prabhu S. Optimization of friction and wear behaviour of Al–Si3N4 nano composite and Al–Gr–Si3N4 hybrid composite under dry sliding conditions. Transactions of Nonferrous Metals Society of China 2017; 27(5): 986-997.

[23] Pasha MB, Kaleemulla M. Processing and characterisation of aluminum metal matrix composites: An overview. Reviews on Advanced Materials Science 2018; 56(1): 79-90.

[24] Gautam G, Mohan A. Effect of ZrB2 particles on the microstructure and mechanical properties of hybrid (ZrB2+Al3Zr)/AA5052 in-situ composites. Journal of Alloys and Compounds 2015; 649: 174-183.

[25] Nai SM, Gupta M, Lim CY. Synthesis and wear characterisation of Al based, free standing functionally graded materials: effects of different matrix compositions. Composites Science and Technology 2003; 63(13): 1895-1909.

[26] Radhika N, Sam M. Enhancement of tribological performance of centrifuge cast functionally graded Cu–10Sn–5Ni alloy with ceramic reinforcements. Journal of Materials Research and Technology 2019; 8(4): 3415-3423.

[27] Dev S, Aherwar A, Patnaik A. Preliminary evaluations on development of recycled porcelain reinforced LM-26/Al-Si10Cu3Mg1 alloy for piston materials. Silicon 2019; 11(3): 1557-1573.

[28] Radhika N, Raghu R. Study on three-body abrasive wear behavior of functionally graded Al/TiB2 composite using response surface methodology. Particulate Science and Technology 2018; 36(7): 816-823.

[29] Ambigai R, Prabhu S. Experimental and ANOVA analysis on tribological behavior of Al/B4C micro and nanocomposite. Australian Journal of Mechanical Engineering 2019; 17(2): 53-63.

[30] Naebe M, Shirvanimoghaddam K. Functionally graded materials: A review of fabrication and properties. Applied Materials Today 2016; 5: 223-45.

[31] Radhika N, Raghu R. Evaluation of dry sliding wear characteristics of LM13 Al/B4C composites. Tribology in Industry 2015; 37(1): 20-28.

[32] Zhang L, He XB, Qu XH, Duan BH, Lu X, Qin ML. Dry sliding wear properties of high volume fraction SiCp/Cu composites produced by pressureless infiltration. Wear 2008; 265: 1848-1856.